Journal of Power Sources 240 (2013) 168–177

Contents lists available at SciVerse ScienceDirect

Journal of Power Sources

journal homepage: www.elsevier.com/locate/jpowsour

Chemical bulk diffusion coefficient of $Sm_{0.5}Sr_{0.5}CoO_{3-\delta}$ cathode for solid oxide fuel cells

Yen-Pei Fu [a,*], Jie Ouyang [a], Chien-Hung Li [a], Shao-Hua Hu [b]

[a] Department of Materials Science and Engineering, National Dong Hwa University, Shou-Feng, Hualien 97401, Taiwan
[b] Department of Environmental Resources Management, Dahan Institute of Technology, Sincheng, Hualien 97145, Taiwan

HIGHLIGHTS

- The oxygen reduction activity is related to the oxygen bulk diffusion properties.
- SDC-infiltrated SSC cathode revealed a decrease in polarization resistance.
- Infiltration method creates extra triple-phase boundaries in cathode backbone.
- D_{chem} was measured by an electrical conductivity relaxation technique.

ARTICLE INFO

Article history:
Received 25 October 2012
Received in revised form
5 January 2013
Accepted 22 March 2013
Available online 2 April 2013

Keywords:
Solid oxide fuel cells
Electrical conductivity relaxation
Chemical diffusion coefficient
Chemical surface exchange coefficient

ABSTRACT

This work reports the characteristics of $Sm_{0.5}Sr_{0.5}CoO_{3-\delta}$ (SSC) cathode including its chemical bulk diffusion coefficient (D_{chem}), current density (i_0), and single cell performance. In this study, the value of D_{chem} is measured by an electrical conductivity relaxation (ECR) technique. The equation of D_{chem} as a function of temperature in the range of 500–700 °C exhibits as follows:

$$D_{chem} = 4.65 \times 10^{-5} \exp\left(-\frac{91.33(\text{kJ mol}^{-1})}{RT}\right)\left(\text{m}^2\ \text{s}^{-1}\right)$$

To improve the cathode performance, the active ionic-conductive $Ce_{0.8}Sm_{0.2}O_{1.9}$ (SDC) nanoparticles deposit on a porous SSC cathode surface by infiltration method. The enhancement in electrochemical performances is ascribed to the creation of electrolyte/cathode phase boundaries, which considerably increases the electrochemical sites for oxygen reduction reaction. In this work, the 0.2 M SDC-infiltrated SSC reveals the maximum peak power density of 489 mW cm^{-2} at operating temperature of 700 °C with a thin film SDC electrolyte (30 μm), a Ni + SDC anode (1 mm) and a SDC-infiltrated SSC cathode (20 μm).

1. Introduction

Recently, solid oxide fuel cells (SOFCs) have attracted a great deal of attention due to the advantages of high electrical efficiency, fuel versatility, low-pollutant emission, etc [1–4]. However, their high operating temperatures limit the application of SOFCs, a lower operating temperature is required in the future applications [5]. Cathodes are important components of SOFCs, and developing new cathodes which perform well at the intermediate temperatures (600–800 °C) is a key step in reducing operating temperatures. Potential cathode candidates have normally been based on mixed oxygen ionic and electronic conducting oxides, which have both high ionic and electronic conductivities. The mixed conductivity extends the active oxygen reduction sites from the typical electrolyte–electrode–gas triple-phase boundaries (TPBs) to the entire cathode surface, therefore greatly reducing the cathode polarization at low operating temperatures [6]. The development of cathode materials with high electrocatalytic activity for oxygen reduction reaction (ORR) at intermediate temperature is great importance and it has received considerable attention during the past decade [7,8]. The cathodic reaction involves the reduction of molecule oxygen to oxygen ion by means of a series of intermediate steps, including gas diffusion, surface adsorption, dissociation, charge transfer and so on [9,10]. Consequently, evaluation of the

* Corresponding author. Tel.: +886 3 863 4209; fax: +886 3 863 4200.
E-mail address: d887503@alumni.nthu.edu.tw (Y.-P. Fu).

0378-7753/$ – see front matter © 2013 Elsevier B.V. All rights reserved.
http://dx.doi.org/10.1016/j.jpowsour.2013.03.138

electrocatalytic activity of the cathode toward oxygen reduction at reduced temperature is very important for SOFCs. The ORR activity of an SOFC cathode is closely related to the surface exchange and oxygen bulk diffusion properties. The detailed information about the surface exchange and oxygen bulk diffusion properties will be helpful in understanding the electrochemical properties to perform as a cathode, as well as in providing further guidance on performance optimization [11]. There are several techniques that can be applied to determine the surface exchange and bulk diffusion coefficients of a mixed conductor, such as oxygen permeation measurements, coulometric titrations, electrochemical impedance spectroscopy, oxygen isotope exchange depth profiling (IEDP) using secondary ion mass spectrometry (SIMS), oxygen isotope exchange using mass spectrometry, and relaxation techniques. The electrical conductivity relaxation (ECR) method has turned out to be a facile way to measure the chemical bulk diffusion coefficient (D_{chem}) and chemical surface exchange coefficient (k_{chem}) of a mixed conductor due to the high sensitivity of electrical conductivity to changes in oxygen concentration or oxygen partial pressure [12–17].

Recently, rare earth-doped cobaltite has attracted much attention due to its mixed-conduction characteristics and its relatively high ionic conductivity. Strontium-doped-samarium-cobalite materials ($Sm_{0.5}Sr_{0.5}CoO_3$, SSC) show high conductivity, up to 10^3 S cm^{-1} [18]. Therefore, SSC was selected as the cathode for investigating their ORR activity. In the present study, the D_{chem} of SSC-based materials at various temperatures and oxygen partial pressures was examined by an ECR method. The chemical diffusion coefficient of SSC was calculated from the Arrhenius plots of D_{chem} vs. 1000/T in the temperature range of 500–700 °C.

To improve the cathode performance of SSC, one commonly used method is mixture of a high ionic-conductive second phase like $Ce_{0.8}Sm_{0.2}O_{1.9}$ (SDC) within the cathode. Such a composite cathode can extent the electrochemically active TPBs, where the ORR occurs, and thus improve the electrochemical property [19]. In this study, the active ionic-conductive SDC nanoparticles deposited on a porous SSC cathode surface by infiltration or impregnation could provide a larger number of ORR sites and improving the electrochemical performance leading relatively low area specific resistances [20–23]. The microstructure and electrochemical performance of $Sm_{0.5}Sr_{0.5}Co_0O_{3-\delta}$ cathode with different infiltration parameters were also investigated systematically.

2. Experimental

2.1. Cathode and electrolyte materials preparation

$Sm_{0.5}Sr_{0.5}CoO_{3-\delta}$ (SSC) cathode powders were synthesized by a conventional solid-state reaction synthesis method with high purity Sm_2O_3, $SrCO_3$, and CoO, powders (>99%) as starting materials. These powders were mixed under ethanol and milled for 12 h using zirconia balls. The ball-milled mixture was dried and ground into a powder with mortar and pestle and then calcined in air at 1000 °C for 4 h. The cathode powders were pelletized with a small amount of PVA as binder with an applied uniaxial pressure of 1000 kgf cm^{-2}. SSC was sintered in air at 1300 °C for 4 h with a programmed heating rate of 5 °C min^{-1}. The sintered samples were made up over 95% of the theoretical density in all the specimens for electrical conductivity measuring with different oxygen atmosphere. The $Ce_{0.8}Sm_{0.2}O_{1.9}$ (SDC) powder was synthesized by coprecipitation using $Ce(NO_3)_3\cdot 6H_2O$ and $Sm(NO_3)_3\cdot 6H_2O$ as the starting materials. These starting materials with stoichiometric ratio were dissolved in distilled water and then added to a solution of ammonia. The mixture solution was adjusted to a pH value in the range of 9.5–10. The resultant precipitate was filtered in a vacuum, and washed three times with water and ethanol, respectively. Then, the coprecipitation powder was calcined in air at 600 °C for 2 h. The SDC powder samples were pelletized with a small amount of PVA as binder with an applied unaxial pressure of 1000 kgf cm^{-2} and the dimensions of 15 mm in diameter and 1 mm in thickness. The disc samples were then finally sintered at 1500 °C for 5 h with a programmed heating rate of 5 °C min^{-1} [24].

Aqueous nitrate solution of SDC precursors with different concentration (0.1, 0.2, 0.3 M) were prepared by dissolving proper amount of $Ce(NO_3)_3\cdot 6H_2O$ and $Sm(NO_3)_3\cdot 6H_2O$ in water. Ethyl glycol (EG) was also added to the solution as a complex agent to form the correct phase. Ethanol was added into the aqueous solution with a ration of 1:1 to improve the wetting ability on the SSC backbone. Three microliters of this solution were infiltrated into each side of the porous SSC cathode using a micro-liter syringe in order to control the amount of loading. After allowing the solution to dry in air, the infiltrated cell was fired at 900 °C for 2 h to obtain the desired SDC nanoparticles within the SSC skeleton.

2.2. Electrical conductivity relaxation

The time dependence of the conductivity was measured using the four-probe DC technique, and was recorded by a Keithley 2420 source meter. Measurements were performed on a specimen with a rectangle geometry, having typical size of $5 \times 5 \times 10$ mm^3 and above 95% of the theoretical density over the temperature range of 500–700 °C at an interval of 50 °C. After each temperature change, the bar was stabilized for at least 30 min. A sudden change in the oxygen partial pressure (P_{O_2}), from 0.05 to 0.21 atm was caused by introducing standard gas mixtures of Ar and O_2. Small oxidation and reduction steps were alternatively applied to study the D_{chem}. Typically, a sequence of several reduction/oxidation cycles was performed at each temperature. The electrical conductivity relaxation curve was plotted as $g(t)$ versus t, which was fit by a least square method to an analytical solution of Eq. (1). Either D_{chem} or k_{chem} was the variable fitting parameters [25].

2.3. Symmetrical cell and the single cell fabrication

The working electrode (WE) was prepared by infiltration of nanosized SDC into SSC. The cathode paste consisted of cathode powder, solvent, binder, and plasticizer. The cathode paste was applied on both sides of SDC electrolyte discs with circle patterns using the screen-printing method with a diameter of 13 mm and a thickness of 1 mm. On one side, the cathode paste was painted as the WE with a surface area of 0.385 cm^2. The Pt reference electrode (RE) was located about 0.3–0.4 cm away from the WE. Such a distance was chosen to avoid measurement errors due to the misalignment of the working and counter electrodes. The Pt counter electrode (CE) was arranged on the other side of the SDC disk. After the cathode material was painted on the electrolyte, it was then sintered at 1000 °C for 4 h in air.

In order to evaluate the effect of the concentration of SDC infiltration on the cathode performance in a single cell, the anode-supported fuel cells were prepared. Anode substrates consisting of 58 wt% NiO, 38 wt% SDC and 4 wt% graphite were prepared by a die-pressing process. SDC nanopowders were then added onto the pre-pressed green NiO–SDC substrate. And then, the SDC powders and NiO–SDC substrate were co-pressed to form a green bilayer and subsequently co-sintered at 1400 °C for 4 h to form dense SDC electrolyte. The cathode paste consisted of SSC cathode powder, solvent, binder, and plasticizer was screen-printed onto the SDC electrolyte film supported by NiO–SDC anode and sintered at 1000 °C for 4 h. In order to obtain SDC-infiltrated single cell, nano-structured SDC was infiltrated into SSC cathode backbones. Finally,

the infiltration cell was fired at 900 °C for 2 h to obtain the desired SDC phase.

2.4. Electrochemical and the single cell measurements

The symmetrical testing cell experiments were carried out by using the VoltaLab PGZ301 potentionistat over temperatures ranging from 600 to 800 °C at intervals of 50 °C in a furnace under various oxygen partial pressures. The frequency applied for AC impedance measurements ranged from 100 kHz to 0.1 Hz with 10 mV AC signal amplitude. The electrochemical impedance spectroscopy (EIS) fitting analysis was performed with Zview software. Button cells with and without the infiltration of SDC were measured with humidified hydrogen (3 vol% H_2O) as fuel and air as oxidants to evaluate the performance of the fabricated anode-supported solid oxide fuel cells. The current–voltage characteristics of the single cells were measured at the temperature range of 500–800 °C at intervals of 100 °C.

2.5. Material characterization

The sintered cathodes were characterized by X-ray powder diffractometer (XRD; Rigaku D/MAX-2500 V), with a scanning rate of 4° min^{-1} and a scanning range of 20–80° using a Cu K_α(1.5418 Å) radiation source. The morphologies of nanosized SDC-infiltrated SSC cathodes were measured by scanning electron microscopy (SEM; Hitachi 3500H).

3. Results and discussions

3.1. Structure compatibility with SDC electrolyte

The investigation of the solid-state reactions between SSC and SDC phases is very important for evaluating the cathode polarization resistance of SSC + SDC composite cathode. As shown in Fig. 1, the XRD patterns of 50 wt.% SSC + 50 wt.% SDC calcined at various temperatures, SSC contains a perovskite structure, while SDC contains a cubic fluorite-type structure, the characteristic peaks of both SSC and SDC are clearly separated for the mixture calcined from 900 to 1100 °C. In general, an electrolyte-infiltrated cathode material sintered at a high temperature with a larger grain size of electrolyte that adhered on cathode leads to a decrease in the electrode surface area–gas solid interface (triple-phase boundary, TPB), which results in high polarization resistance [26,27]. Meanwhile, due to the high sintering temperature, the cathode materials adhere strongly to the electrolyte surface, resulting in better contact with the electrolyte and better current collection. This represents a trade-off relationship with regard to the sintering temperature to obtain cathode materials with fine microstructure and strong adhesion to the electrolyte [28]. The results reveal that no obvious interface reaction appeared for the mixture of SSC + SDC from 900 to 1100 °C, indicating the mixture of SSC + SDC was a chemically stable, when heated up to 1100 °C. Similar results were reported by Xia et al. who found that secondary phases were presented when SSC with 10 wt% SDC composite was calcined at 1250 °C for 4 h [29]. This suggests that a solid-state reaction might have taken place between the SSC and SDC phases above 1250 °C. Therefore, the calcination temperature of the symmetrical fuel cell was selected at 900 °C to obtain the desired performance in this study.

3.2. Chemical diffusion coefficient (D_{chem})

The electrode performance is closely related to the intrinsic properties of the electrode material, such as surface exchange kinetics and bulk diffusion properties. In this study, D_{chem} or k_{chem} can be measured by an electrical conductivity relaxation (ECR) technique, which is based on the principle that a variation in the ambient atmosphere leads to a change in the oxygen vacancy concentration of the mixed ionic and electronic conductor (MIEC). Due to the local electroneutrality requirement, the abrupt change in the P_{O_2} of the surrounding atmosphere induces a corresponding change of the charge carrier concentration (oxygen vacancy), which is reflected as a relaxation of the apparent macroscopic electrical conductivity [30]. This relaxation process is accompanied by oxygen exchange at the surface and chemical diffusion in the bulk of the oxide sample. Conductivity relaxation models usually assume small departures from thermal equilibrium and a simple linear model for the surface exchange kinetics [31,32]. Fig. 2 shows the electrical conductivity relaxation curves of SSC at various temperatures by a sudden change in the P_{O_2} from 0.21 to 0.05 atm. The values for k_{chem} or D_{chem} could be obtained by fitting the electrical conductivity relaxation curves into Eq. (1). SSC cathode in the reduction process was given in Table 1.

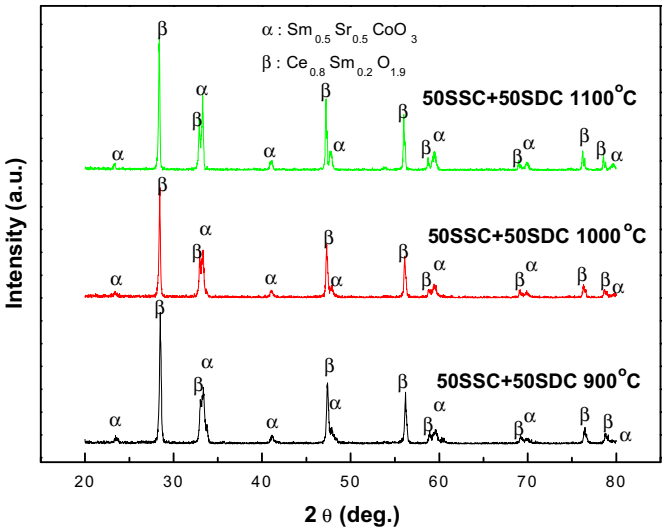

Fig. 1. X-ray diffraction pattern of the powder mixture of 50 wt.% SSC + 50 wt.% SDC calcined at (a) 900 °C, (b) 1000 °C, and (c) 1100 °C for 4 h.

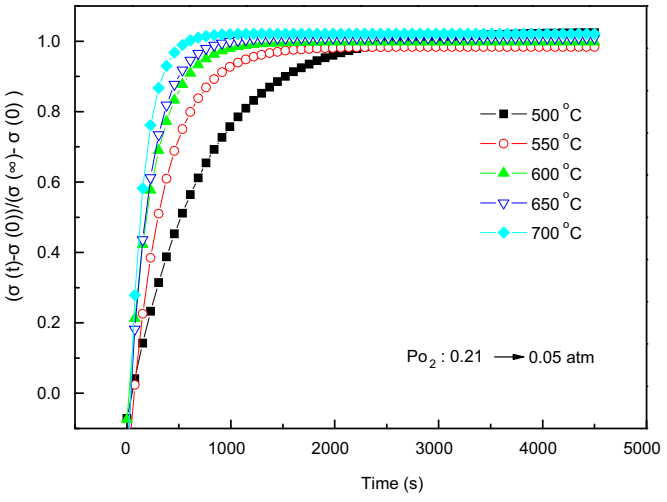

Fig. 2. The electrical conductivity relaxation curve for SSC at various temperatures after the oxygen pressure suddenly changed from 0.21 to 0.05 atm.

Table 1
D_{chem} of SSC at various temperatures from electrical conductivity relaxation curve during the oxygen partial pressure suddenly changed from 0.21 to 0.05 atm.

Temperature (°C)	D_{chem} ($cm^2 s^{-1}$)
500	1.56×10^{-6}
550	9.38×10^{-6}
600	1.74×10^{-5}
650	2.29×10^{-5}
700	3.63×10^{-5}

$$\frac{\sigma(t)-\sigma(0)}{\sigma(\infty)-\sigma(0)} = 1 - \sum_{n=1}^{\infty}\sum_{m=1}^{\infty}\sum_{p=1}^{\infty} \times \frac{2C_1^2 \exp\left(-\alpha_{1n}^2 D_{chem} t/l_1^2\right)}{\alpha_{1n}^2\left(\alpha_{1n}^2 + C_1^2 + C_1\right)} \times \frac{2C_2^2 \exp\left(-\alpha_{2m}^2 D_{chem} t/l_2^2\right)}{\alpha_{2m}^2\left(\alpha_{2m}^2 + C_2^2 + C_2\right)} \times \frac{2C_3^2 \exp\left(-\alpha_{3p}^2 D_{chem} t/l_3^2\right)}{\alpha_{3p}^2\left(\alpha_{3p}^2 + C_3^2 + C_3\right)} \quad (1)$$

where D_{chem} is the chemical diffusion coefficient, and $\sigma(0)$, $\sigma(t)$, and $\sigma(\infty)$ indicate the initial, time independent and final conductivities, respectively. The coefficients of α_{1n}, α_{2m}, α_{3p} are the nth, mth and pth roots of the transcendental equations:

$$C_1 = \alpha_{1n}\tan\alpha_{1n}, C_2 = \alpha_{2m}\tan\alpha_{2m}, C_3 = \alpha_{3p}\tan\alpha_{3p} \quad (2)$$

The parameters of C_1, C_2, and C_3 are defined as:

$$C_1 = \frac{l_1}{L_d}, C_2 = \frac{l_2}{L_d}, C_3 = \frac{l_3}{L_d}, L_d = \frac{D_{chem}}{k_{ex}} \quad (3)$$

where k_{chem} is the surface exchange coefficient in the relaxation process.

The conductivity reached its steady state value faster for the high temperatures than the low temperatures, leading to the fact that D_{chem} at high temperatures was larger than one at low temperatures. D_{chem} for SSC were 0.16×10^{-5}, 1.74×10^{-5}, and 3.63×10^{-5} $cm^2 s^{-1}$ at 500, 600, and 700 °C, respectively. The activation energies for D_{chem} obtained from the slopes of the Arrhenius plots as shown in Fig. 3 were 91 kJ mol^{-1}. The D_{chem} measured in this work is in the same order of magnitude to those measured by Huang et al. [25]. The variance between the previous paper and this work is ascribed to the different procedure applied during the ECR measurement. The equation of D_{chem} as a function of temperature calculated from the Arrhenius plots of D_{chem} vs. 1000/T exhibits as follows:

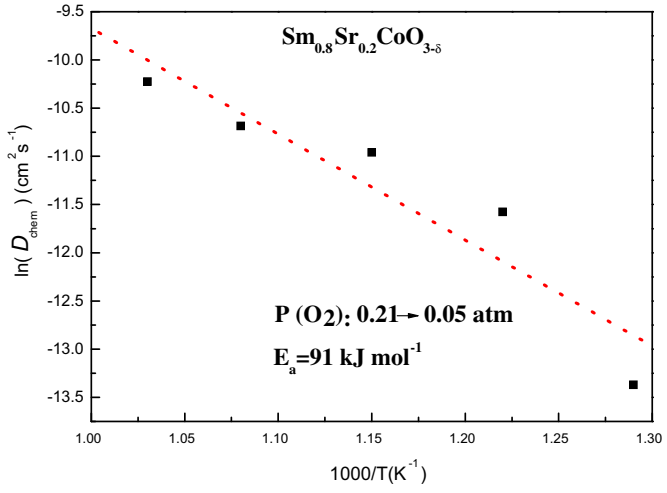

Fig. 3. Arrhenius plots of D_{chem} vs. 1000/T for SSC cathode between 500 and 700 °C.

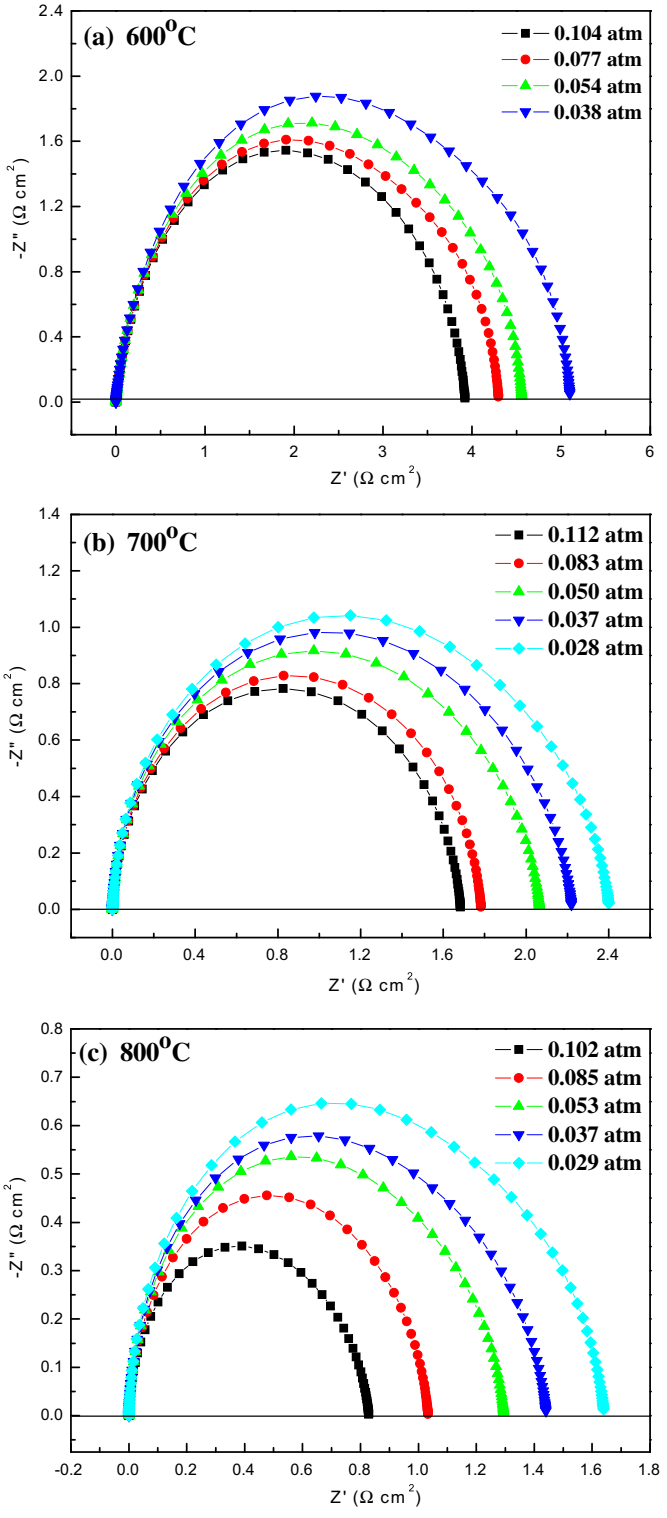

Fig. 4. Nyquist diagram of the impedance spectroscopy for SSC cathode on SDC electrolyte with various oxygen partial pressures at (a) 600 °C; (b) 700 °C; and (c) 800 °C, respectively.

$$D_{\text{chem}} = 4.65 \times 10^{-5} \exp\left(-\frac{91.33\,(\text{kJ mol}^{-1})}{RT}\right)(\text{m}^2\ \text{s}^{-1}) \quad (4)$$

This equation is applied in the temperature range of 500–700 °C. The activation energy obtained from the Arrhenius plot of D_{chem} may be considered in terms of the enthalpy of mobility of the defects involved in the gas/solid equilibration for the $O_2/Sm_{0.5}Sr_{0.5}CoO_3$ system. This effect is considered in terms of the effect of oxygen partial pressure and related concentration of defects, on the extent of interactions between the defects and their mobility [33].

3.3. Oxygen partial pressure related impedance spectrum

The impedance spectra could be separated from two arcs indicating that the oxygen reduction reaction between the interface of cathode and electrolyte could be composed of two different processes. The interfacial polarization resistance at the high frequency (R_{HF}) is probably associated with charge transfer processes, including the electron-transfer and ion transfer processes occurring at the current collector/cathode electrode and cathode electrode/electrolyte interfaces, respectively. The interfacial polarization resistance at the low frequency (R_{LF}) can be attributed to the diffusion processes, which include adsorption–desorption of oxygen, oxygen diffusion at the gas–cathode surface interface, and surface diffusion of intermediate oxygen species [34–37]. Generally, the interfacial polarization resistance (R_{P}) changes with P_{O_2} can be described by the following equation:

$$R_{\text{p}} = R_{\text{p}}^{0}(P_{O_2})^{-n} \quad (5)$$

The magnitude of n provides valuable information about the type of species involved in the oxygen reduction reactions [38,39]:

$$n = 0.25, O_{\text{ads.}} + 2e' + V_{\text{O}}'' \Leftrightarrow O_{\text{O}}^{x} \quad (6)$$

$$n = 0.50, O_{2,\ \text{ads.}} \Leftrightarrow 2O_{\text{ads.}} \quad (7)$$

$$n = 1.00, O_2(\text{g}) \Leftrightarrow O_{2,\ \text{ads.}} \quad (8)$$

where $n = 0.25$ has been associated with the charge transfer processes, $n = 0.50$ with oxygen adsorption/desorption processes, and $n = 1.00$ with gas phase diffusion of oxygen molecules in a porous cathode. Nyquist diagrams of the impedance spectroscopy for SSC cathode at 600, 700, and 800 °C with various oxygen partial pressures were shown in Fig. 4. Noticeably, the R_{P} increased with decreasing P_{O_2}. The R_{HF} as a function of P_{O_2} for SSC cathode measured at various temperatures is shown in Fig. 5(a). With increasing temperature, the slopes of log(R_{P}) vs. log(P_{O2}) plot increased from operating temperature of 600 °C of the value of $n = 0.13$ to 800 °C of the value of $n = 0.21$, which indicated that the mechanism of ORR is gradually dominated by the electron-transfer process. The interfacial polarization resistances at the R_{LF} as a function of P_{O_2} measured at various temperatures are shown in Fig. 5(b). With increasing temperature, the slopes for log(R_{P}) vs. log(P_{O2}) plot gradually increased from operating temperature of 600 °C of the value of $n = 0.25$ to 800 °C of the value of $n = 0.50$, indicating that the mechanism of ORR may gradually transfer from electron-transfer process to oxygen adsorption/desorption processes.

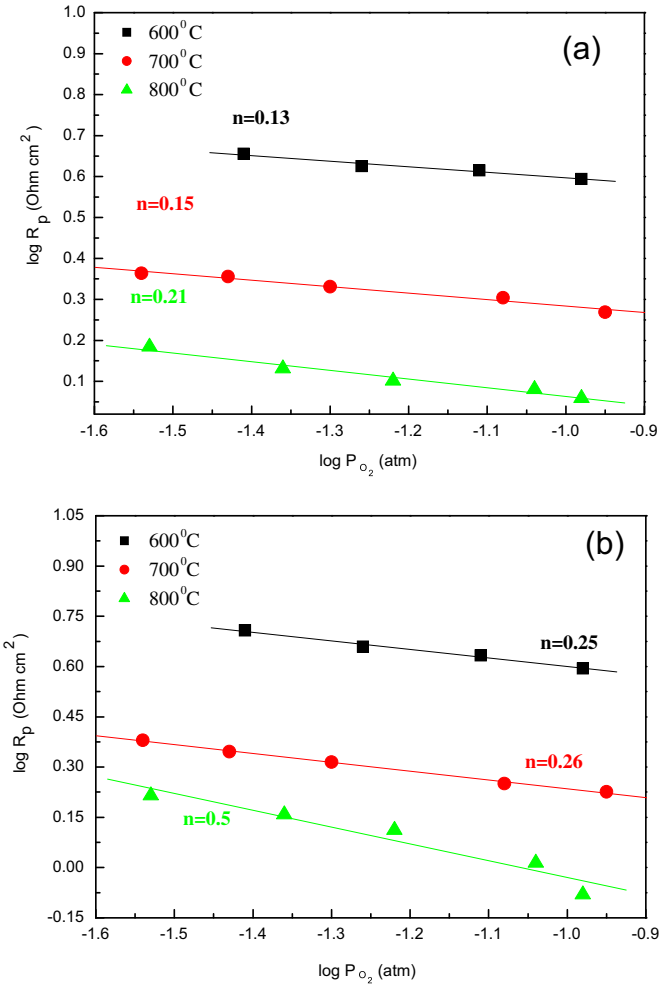

Fig. 5. The interfacial polarization resistance at (a) high frequency (R_{HF}) and (b) low frequency (R_{LF}) as a function of oxygen partial pressure for SSC cathode measured in the temperature range of 600–800 °C.

3.4. SEM of SSC infiltrated with SDC

To improve the cathode performance, the active ionic-conductive SDC nanoparticles were deposited on a porous SSC cathode surface by infiltration method in this study. The microstructures of the SSC cathode infiltrated with various concentrations of SDC were observed by SEM as shown in Fig. 6. In this study, to improve the wetting ability between the nitrate solution of SDC precursors and the porous SSC backbones, a mixture of ethanol and water was used in all specimens. Fig. 6(a) shows the microstructure of SSC cathode, which revealed that SSC backbone was well sintered without any tiny SDC particles. After infiltrating with 3 μl of 0.1 M SDC, nanosize SDC particles with tiny grain size in the range of 10–30 nm were introduced to the SSC backbone as shown in Fig. 6(b). As the concentration of SDC was increased from 0.1 M to 0.2 M, uniformly distributed SDC nanoparticles were observed on the surface of SSC grains with a relative narrow size distribution in the range of 30–40 nm a shown in Fig 6(c). When the concentration further increased to 0.3 M, both number and size of nanoparticles were increased and the average particle size of about 70 nm. Noticeably, the grain size of SDC particles formed on the porous SSC backbones increased with the concentration of SDC.

3.5. Interfacial polarization resistances

The morphologies of SDC particles formed on the porous SSC backbones and the concentrations of SDC infiltration greatly

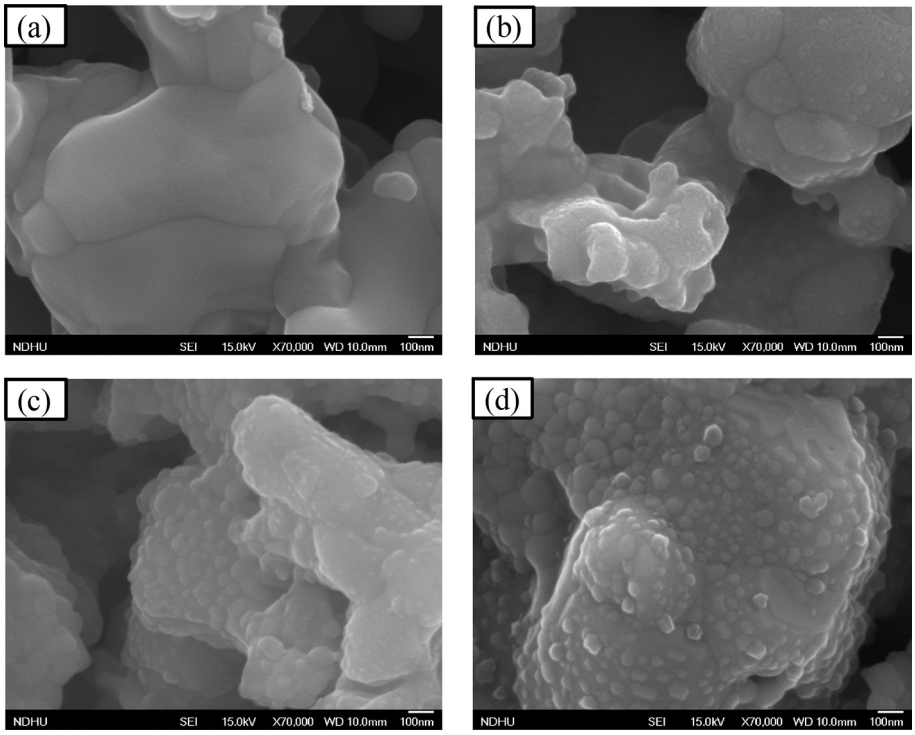

Fig. 6. SEM images of (a) SSC; (b) 0.1 M SDC-infiltrated SSC; (c) 0.2 M SDC-infiltrated SSC; and (d) 0.3 M SDC-infiltrated SSC, respectively.

influence the electrochemical performance of the infiltrated cathodes. Fig. 7 shows some typical impedance spectra of the SSC cathode infiltrated with various concentrations of SDC measured in a symmetric configuration using AC impedance spectroscopy under open-circuit conditions in air from 600–800 °C at the interval of 50 °C. In order to clearly show the difference in the cathode polarization behavior between the Ohmic resistance (R_Ω) and the total cathode polarization resistance (R_P) of the cell, the R_Ω was eliminated in the impedance plot. The catalytic activity of the SSC cathodes, as characterized by the R_P, was determined from the size of the impedance loop [40]. It was apparent that the SSC cathode infiltrated with SDC revealed a significant reduction in R_P. The detailed fitting parameters of SSC cathode were listed in Table 2. The R_p values of SSC without infiltrated with SDC were 1.940, 0.473, and 0.151 Ω cm^2 at 600, 700, and 800 °C, respectively. When 0.1 M SDC infiltrated into the SSC cathode, the R_p values were reduced to 0.581, 0.125, and 0.027 Ω cm^2 at 600, 700, and 800 °C, respectively. As the concentration of SDC was increased to 0.2 M, the R_p values were further reduced to 0.547, 0.090, and 0.026 Ω cm^2 at 600, 700, and 800 °C, respectively. After infiltration, the impedance spectrum shape seemingly changed that both high- and low-frequency arcs were obviously reduced. It indicated that both electrochemical processes (i.e. the electrochemical reactions at the electrode–electrolyte interface and adsorption–desorption of oxygen, oxygen diffusion at the gas-cathode surface interface.) were simultaneously improved by active SDC nanoparticles deposited on SSC cathode backbone. The dramatic decrease in R_p was mainly attributed to the creation of SDC/SSC phase boundaries. The newly formed SDC deposited on the SSC cathode with highly porous skeleton would allow gas-phase molecules to easily diffuse to the SDC/SSC boundaries, which considerably increased the electrochemical sites for oxygen reduction reaction (ORR) [41]. The ORR sites were not only at the real SSC cathode surface area simultaneously exposed to electrolyte and air, but also at these newly formed SDC nanoparticles deposited on SSC porous skeleton. Nevertheless, when the concentration of the SDC solution was increased to 0.3 M, the values of R_p were slightly greater than those of 0.2 M. It was presumed that the SDC nanoparticles precipitated too much on SSC porous skeleton, reducing gas-phase molecules to diffuse to the SSC/SDC boundaries.

3.6. The exchange current density (i_0)

The exchange current density, i_0, which corresponds to the intrinsic ORR rate, is an important parameter for investigating ORR mechanisms at the cathode [42]. In general, the ORR can be divided into several elemental steps: (1) diffusion of oxygen molecules in the gas phase to the electrode, (2) oxygen dissociate adsorption on the cathode surface, (3) surface diffusion of oxygen on the cathode, (4) incorporation of oxygen into the electrolyte via the TPBs, and (5) oxide ion diffusion in the bulk of the cathode, and oxide ion transfer from cathode to electrolyte [43,44]. When the i_0 values are higher, the overpotentials of the cathode are lower, suggesting that cathodes with high i_0 values exhibit high performance in terms of electrochemical properties. The i_0 value can be obtained from the AC impedance measurement (EIS). In this technique, i_0 was measured from the polarization resistance, R_p, of the Nyquist plot and calculated using Eq. (1) which is derived from the Bulter–Volmer equation [45]:

$$i_0 = \frac{RT\nu}{nFR_p} \tag{9}$$

Here n is the total number of electrons passed in the reaction, ν reflects the number of times the rate-determining step occurs for one occurrence of the full reaction, F is the Faraday constant ($F = 96{,}500$ C mol^{-1}), and R is the ideal gas constant ($R = 8.31$ J mol^{-1} K^{-1}). For the ORR, n and ν are generally assumed to be 4 and 1, respectively (as the total number of electrons transferred per molecule of oxygen reduced is 4 and the rate-limiting

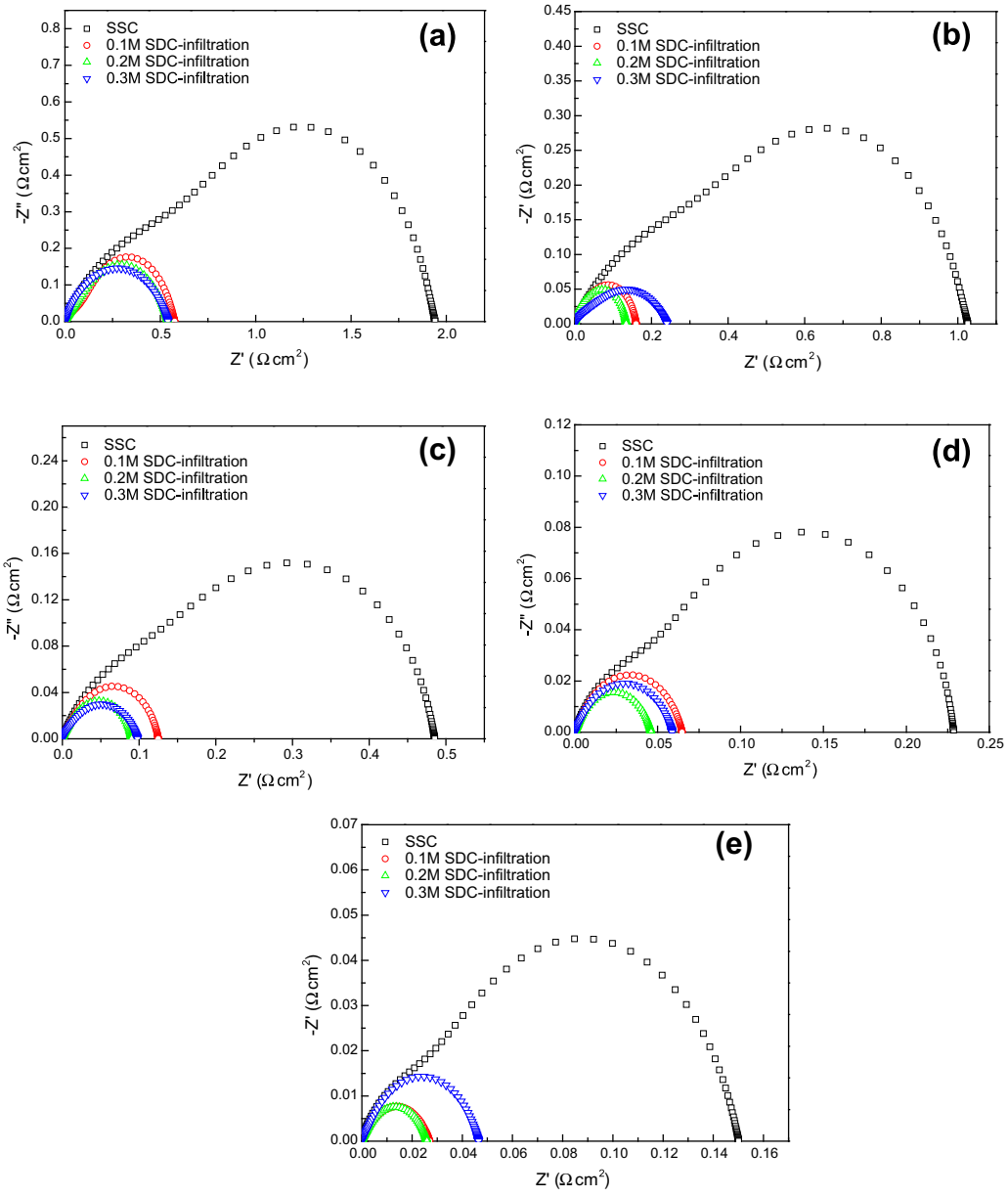

Fig. 7. (a) Impedance spectra of SSC cathode infiltrated with various concentrations of SDC at various temperatures: (a) 600 °C; (b) 650 °C; (c) 700 °C; (d) 750 °C; and (e) 800 °C, respectively.

step would likely have a stoichiometry of 1 for the ORR) [46]. The i_0 values for the different cathode-half-cell configurations measured from Eq. (9) for EIS are given in Table 3, and their Arrhenius plots for i_0 values as a function of temperature are shown in Fig. 8. The i_0 values of SSC without infiltrated with SDC were 10.6, 94.8, and 491.8 mA cm^{-2} at 600, 700, and 800 °C, respectively. When 0.1 M SDC infiltrated into the SSC cathode, the i_0 values were increased to 32.4, 167.7, and 850.0 mA cm^{-2} at 600, 700, and 800 °C, respectively. As the concentration of SDC was increased to 0.2 M, the i_0 values were further increased to 34.4, 232.1, and 885.6 mA cm^{-2} at 600, 700, and 800 °C, respectively. Nevertheless, when the

Table 2
Results of the fitting parameters of SSC cathode infiltrated with different concentrations of SDC at various temperatures.

SDC concentration (M)	R_P (Ω cm^2)				
	600 °C	650 °C	700 °C	750 °C	800 °C
SSC	1.940	1.031	0.473	0.231	0.151
0.1	0.581	0.161	0.125	0.064	0.027
0.2	0.547	0.134	0.090	0.046	0.026
0.3	0.541	0.242	0.098	0.058	0.046

Table 3
Exchange current density (i_0) measured from EIS technique for the SSC cathode infiltrated with different concentrations of SDC in the temperature range of 600–800 °C.

T (°C)	i_0 (mA cm^{-2})			
	SSC	0.1 M SDC	0.2 M SDC	0.3 M SDC
600 °C	10.6	32.4	34.4	34.7
650 °C	31.0	124.3	148.4	82.2
700 °C	94.8	167.7	232.1	213.9
750 °C	225.3	340.0	477.8	374.9
800 °C	491.8	850.0	885.6	496.4

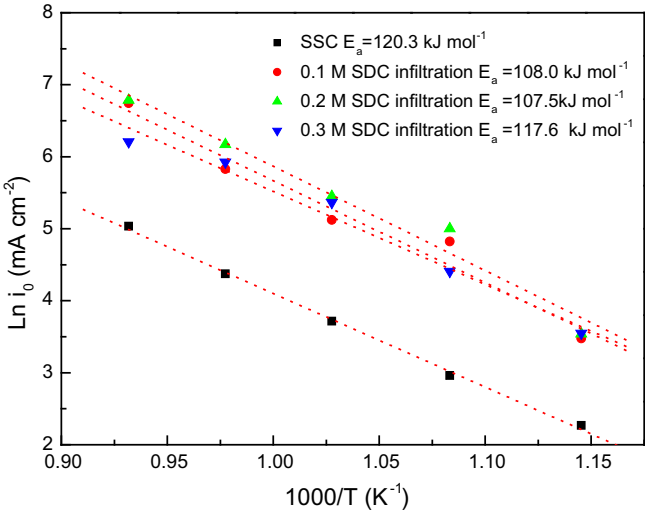

Fig. 8. Arrhenius plots of oxygen reduction reaction for SSC cathode infiltrated with various concentrations of SDC, in which i_0 values obtained using EIS technique.

concentration of the SDC solution was increased to 0.3 M, the i_0 values were 34.7, 213.9, and 496.4 mA cm^{-2} at 600, 700, and 800 °C, respectively. When 0.1 M SDC infiltrated into the SSC cathode, the newly formed SDC deposited on the SSC porous skeleton which sites could take place electrochemical reaction for ORR, this reason made the i_0 values increasing. However, when the concentration of the SDC was increased to 0.3 M, the i_0 values gradually decreased than those for the SSC infiltrated with 0.1 M. It was speculated that the large amount of SDC nanoparticles precipitated on SSC porous skeleton, reducing oxygen gas-phase molecules to diffuse to the SSC/SDC boundaries where the sites took place ORR. From the slope of the line in the Arrhenius plots, the overall activation energy for the ORR was determined by the following equation.

$$\ln i_0 = \ln K - \frac{E_a}{RT} \quad (10)$$

where K is the pre-exponential constant, which can be calculated from the y-intercept, and E_a is the reaction activation energy [47]. The difference in E_a for the ORR may be related to several factors such as the (1) different cathode preparation methods, (2) structure of the cathode, or (3) different cathode compositions. Nevertheless, in this study, the E_a for the ORR is directly related to the structure of the cathode. The E_a for the ORR obtained from the slopes of the Arrhenius plots were 108.0, 107.5, and 117.6 kJ mol^{-1} for SSC cathode infiltrated with 0.1, 0.2, and 0.3 M SDC, respectively. As for the E_a of the SSC cathode without infiltrated with SDC was 120.31 kJ mol^{-1}. This behavior suggested that the infiltration of electrolyte nanopowders on porous skeleton cathode significantly improved the electrochemical properties of cathode.

3.7. Single cell performance

To evaluate the cathodic performance of SSC infiltrated with SDC nanoparticles, an anode-supported single fuel cell with a thin film SDC electrolyte (30 μm), a Ni + SDC anode (1 mm) and a SDC-infiltrated SSC cathode (20 μm) were fabricated. The performance (including *I–V* curve and *I–P* curve under different operating

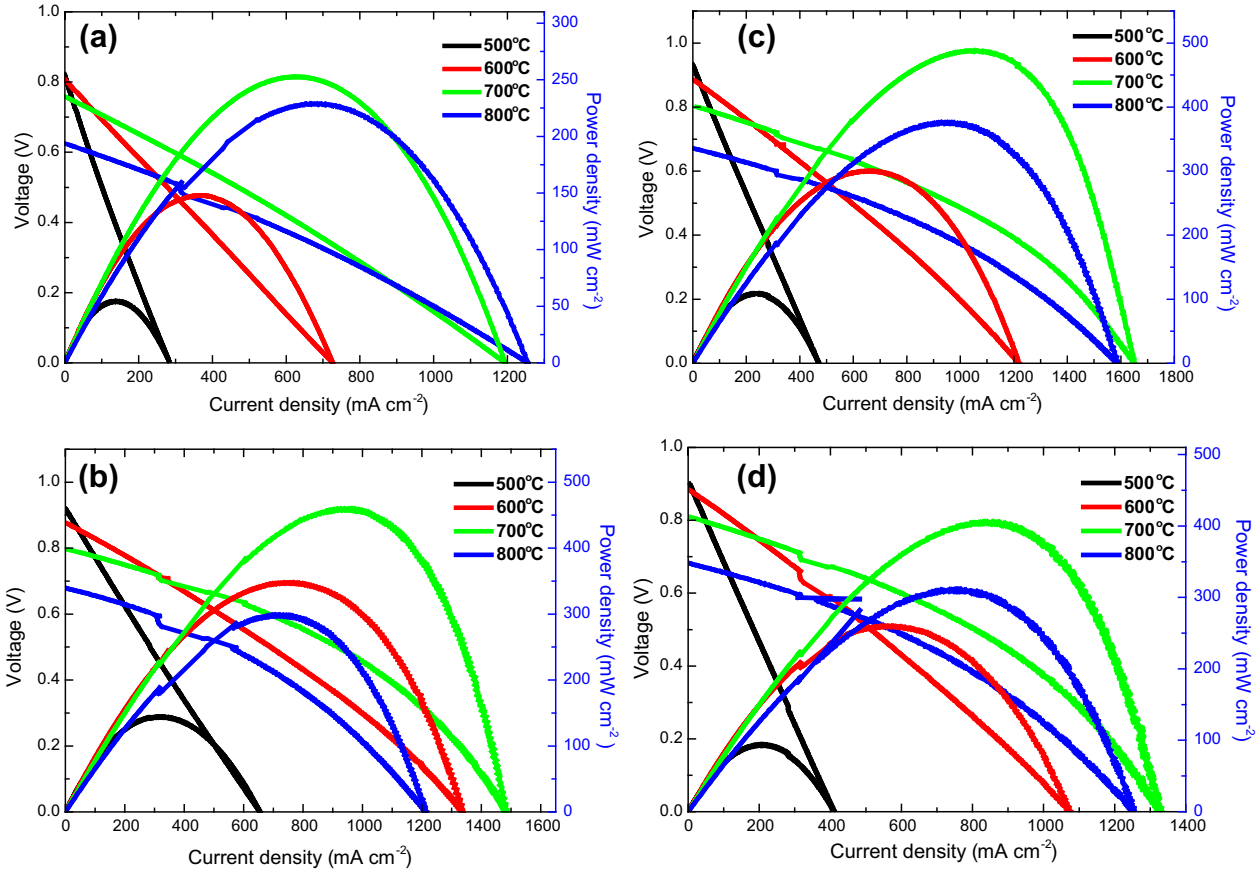

Fig. 9. The *I–V* and *I–P* curves for SOFCs with a SSC cathode infiltrated with various concentration of SDC: (a) no SDC; (b) 0.1 M SDC; (c) 0.2 M SDC; and (d) 0.3 M SDC, respectively.

Table 4
The peak power densities in the temperature range of 500–800 °C of the anode-supported single cells for SSC cathode infiltrated with different concentrations of SDC.

SDC concentration (M)	The peak power density ($mW\,cm^{-2}$)			
	500 °C	600 °C	700 °C	800 °C
SSC	54	148	253	229
0.1	144	348	460	299
0.2	109	300	489	376
0.3	94	259	406	311

temperatures) of the SSC cathode infiltrated with and without SDC in anode-supported SOFCs using SDC as an electrolyte as shown in Fig. 9. Generally, the open-circuit voltage (OCV) of an ideal cell should be close to its theoretic value of 1.1 V, and slightly influenced by the operating condition. In this study, the values of practical OCV were lower than its theoretical value; this might be ascribed to the following reasons. First, the SDC electrolyte possessed minor electronic conductivity, a slight electron cross flow (current leakage) might occur through the electrolyte. Secondly, the electrolyte membrane might be not dense, the fuel/oxidant cross flow could take place. The higher the current leakage exists, the lower the cell OCV will be. As shown in Fig. 9(a) are the current–voltage curves and the corresponding power densities for cells without SDC infiltration at various operating temperatures. The peak power densities of 148, 253, and 229 $mW\,cm^{-2}$ were achieved at 600, 700, and 800 °C, respectively. When 0.1 M SDC infiltrated into the SSC cathode, the peak power densities were increased to 348, 460, and 299 $mW\,cm^{-2}$ at 600, 700, and 800 °C, respectively, as shown in Fig. 9(b). As the concentration of SDC was increased to 0.2 M, the peak power densities were further increased to 300, 489, and 376 $mW\,cm^{-2}$ at 600, 700, and 800 °C, respectively (Fig. 9(c)). However, when the concentration of the SDC solution was increased to 0.3 M, the values of the peak power densities slightly decreased than those for the infiltration of 0.3 M SDC. As shown in Fig. 9(d), the peak power densities were 259, 406, 311 $mW\,cm^{-2}$ at 600, 700, and 800 °C, respectively. With various concentrations of SDC infiltrated into the SSC, the electrochemical properties performance of the anode-supported single cells also changed, and the peak power densities at the temperature range of 500–800 °C were shown in Table 4. It can be seen that the SSC cathode infiltrated with 0.2 M SDC operating at 700 °C demonstrates the highest peak power density of 489 $mW\,cm^{-2}$. This indicates that the infiltration the electrolyte nanoparticles into the porous cathode backbones really improve the electrochemical performance of a single cell. In this study, the infiltration technique was performed to improve the electrochemical properties of cathode. The newly formed electrolyte of SDC nanopowders deposited on the SSC cathode with porous skeleton would allow gas-phase molecules to easily diffuse to the SDC/SSC boundaries where the sites took place ORR. This behavior leads to the considerable increase in the electrochemical sites for ORR and the value of peak power density. However, when the concentration of infiltrated-SDC exceeded a certain value (0.2 M), the gas-phase molecules diffused to the SSC/SDC boundaries were blocked and their electrochemical performance decreases (including the current density and the peak power density).

4. Conclusions

The oxygen reduction activity of an SOFC cathode is closely related to the oxygen bulk diffusion properties. Knowledge about chemical bulk diffusion coefficient (D_{chem}) of mixed conductors would be useful for practical applications. Through the electrical conductivity relaxation test, the values of D_{chem} for SSC were calculated from 0.16×10^{-5} $cm^2\,s^{-1}$ of 500 °C to 3.63×10^{-5} $cm^2\,s^{-1}$ of 700 °C. The activation energie for D_{chem} was 91 $kJ\,mol^{-1}$. The equation of D_{chem} as a function of temperature in the range of 500–700 °C exhibits as follows:

$$D_{chem} = 4.65 \times 10^{-5} \exp\left(-\frac{91.33\,(kJ\,mol^{-1})}{RT}\right)\left(m^2\,s^{-1}\right)$$

To improve the electrochemical properties of cathode, SSC cathodeS coated with SDC electrolyte nanoparticles were prepared by an infiltration method. Based on the experimental results, it is revealed that the microstructure and electrochemical properties of SDC-infiltrated SSC cathode closely depend on the concentration of SDC introduced. For the SSC cathode infiltrated with 3 μL of 0.2 M SDC with optimum peak power density of anode-supported SOFC single cell was 489 $mW\,cm^{-2}$ at 700 °C. The significant increase in electrochemical performances was mainly attributed to the creation of electrolyte/cathode phase boundaries. The newly formed electrolyte nanoparticles deposited on the porous skeleton cathode would allow gas-phase molecules to easily diffuse to the electrolyte/cathode boundaries, increasing the electrochemical sites for oxygen reduction reaction.

Acknowledgments

The authors would like to thank the National Science Council of Taiwan for financially supporting this research under Contract No. NSC 101-2113-M-259-004.

References

[1] K.T. Lee, D.W. Jung, H.S. Yoon, A.A. Lidie, M.A. Camaratta, E.D. Wachsman, J. Power Sources 220 (2012) 324–330.
[2] S. Park, S. Choi, J. Shin, G. Kim, J. Power Sources 210 (2012) 172–177.
[3] Y. Wang, H. Zhang, F. Chen, C. Xia, J. Power Sources 203 (2012) 34–41.
[4] S.C. Singhal, Solid State Ionics 152 (2002) 405–410.
[5] H. Moon, S.D. Kim, S.H. Hyun, S.H. Kim, Int. J. Hydrogen Energy 33 (2008) 1758–1768.
[6] W. Zhou, Z. Shao, R. Ran, P. Zeng, H. Gu, W. Jin, N. Xu, J. Power Sources 168 (2007) 330–337.
[7] Z.P. Shao, S.M. Haile, Nature 431 (2004) 170–173.
[8] W. Zhou, Z.P. Shao, R. Ran, W.Q. Jin, N.P. Xu, Chem. Commun. 44 (2008) 5791–5793.
[9] B.W. Liu, Y. Zhang, L.M. Zhang, Int. J. Hydrogen Energy 34 (2009) 1008–1014.
[10] X.J. Chen, S.H. Chan, K.A. Khor, Electrochim Acta 41 (2004) 1851–1861.
[11] D. Chen, Z. Shao, Int. J. Hydrogen Energy 36 (2011) 6948–6956.
[12] E. Bucher, A. Egger, P. Ried, W. Sitte, P. Holtappels, Solid State Ionics 179 (2008) 1032–1035.
[13] X. Chen, S. Wang, Y.L. Yang, L. Smith, N.J. Wu, B.I. Kim, Solid State Ionics 146 (2002) 405–413.
[14] A. Zomorrodian, H. Salamati, Z.G. Lu, X. Chen, N.J. Wu, A. Ignatiev, Int. J. Hydrogen Energy 35 (2010) 12443–12448.
[15] I. Yasuda, T. Hikita, J. Electrochem. Soc. 141 (1994) 1268–1273.
[16] I. Yasuda, M. Hishinuma, Solid State Ionics 80 (1995) 141–150.
[17] I. Yasuda, M. Hishinuma, J. Solid State Chem. 123 (1996) 382–390.
[18] T. Ishihara, M. Honda, T. Shibayama, H. Minami, H. Nishiguchi, Y. Takita, J. Electrochem. Soc. 145 (1998) 3177–3183.
[19] B. Wei, Z. Lu, T. Wei, D. Jia, X. Huang, Y. Zhang, J. Miao, W. Su, Int. J. Hydrogen Energy 36 (2011) 6151–6159.
[20] Y.Y. Huang, K. Ahn, J.M. Vohs, R.J. Gorte, J. Electrochem. Soc. 151 (2004) A1592–1597.
[21] T.Z. Sholklapper, C. Lu, C.P. Jacobson, S.J. Visco, L.C. De Jonghe, Electrochem. Solid State Lett. 9 (2006) A376–378.
[22] M. Shah, S.A. Barnett, Solid State Ionics 179 (2008) 2059–2064.
[23] J.M. Vohs, R.J. Gorte, Adv. Mater 21 (2009) 943–956.
[24] Y.P. Fu, S.B. Wen, C.H. Lu, J. Am. Ceram. Soc. 91 (2008) 127–131.
[25] C. Huang, D. Chen, Y. Lin, R. Ran, Z. Shao, J. Power Sources 195 (2010) 5176–5184.
[26] H.J. Hwang, J.W. Moon, J. Moon, M. Awano, J. Am. Ceram. Soc. 88 (2005) 79–84.
[27] H.J. Hwang, J.W. Moon, S. Lee, E.A. Lee, J. Power Sources 145 (2005) 243–248.
[28] Y.P. Fu, C.H. Li, S.H. Hu, J. Electrochem. Soc. 159 (2012) B629–634.
[29] C.R. Xia, W. Rauch, F.L. Chen, M.L. Liu, Solid State Ionics 149 (2002) 11–19.
[30] H. Dunwald, C. Wagner, Z. Phys. Chem. B 24 (1934) 53–58.
[31] I. Yasuda, H. Hikita, J. Electrochem. Soc. 141 (1994) 1268–1273.
[32] J.E. Elshof, M.H.R. Lankhorst, H.J.M. Bouwmeester, J. Electrochem. Soc. 144 (1997) 1060–1067.
[33] T. Bak, J. Nowotny, C.C. Sorrel, J. Phys. Chem. Solids 65 (2004) 1229–1241.

[34] W. Zhou, R. Ran, Z. Shao, R. Cai, W. Jin, N. Xu, J. Ahn, Electrochim. Acta 53 (2008) 4370–4380.
[35] S.B. Adler, Solid State Ionics 135 (2000) 603–612.
[36] C. Fu, K. Sun, N. Zhang, X. Chen, D. Zhou, Electrochim. Acta 52 (2007) 4589–4594.
[37] F. Qiang, K.N. Sun, N.Q. Zhang, X.D. Zhu, S.R. Le, D.R. Zhou, J. Power Sources 168 (2007) 338–345.
[38] Y. Takeda, R. Kanno, M. Noda, Y. Tomida, O. Yamamoto, J. Electrochem. Soc. 134 (1987) 2656–2661.
[39] A. Jaiswal, E.D. Wachsman, J. Electrochem. Soc. 152 (2005) A787–790.
[40] L. Nie, M. Liu, Y. Zhang, M. Liu, J. Power Sources 195 (2010) 4704–4708.
[41] S.P. Jiang, Int. J. Hydrogen Energy 37 (2012) 449–470.
[42] S.B. Adler, Chem. Rev. 104 (2004) 4791–4843.
[43] M. Kleitz, F. Petitbon, Solid States Ionics 92 (1996) 65–74.
[44] A. Ringuede, J. Fouletier, Solid States Ionics 139 (2001) 167–177.
[45] J. Piao, K. Sun, N. Zhang, X. Chen, S. Xu, D. Zhou, J. Power Sources 172 (2007) 633–640.
[46] J. Liu, A.C. Co, B. Paulson, V.I. Briss, Solid State Ionics 177 (2006) 377–387.
[47] A.C. Co, S.J. Xia, V.I. Briss, J. Electrochem. Soc. 152 (2005) A570–576.